Analytical Study of ZnO-based HEMT for Power Switching

Pawan Kumar (phd1701202002@iiti.ac.in)
Indian Institute of Technology Indore
Sumit Chaudhary
Indian Institute of Technology Indore
Md Arif Khan
Indian Institute of Technology Indore
Sanjay Kumar
Indian Institute of Technology Indore
Shaibal Mukherjee
Indian Institute of Technology Indore

Research Article

Keywords: Efficiency, power dissipation, MgZnO/ZnO HEMT, 2DEG, switching frequency

Posted Date: December 28th, 2021

DOI: https://doi.org/10.21203/rs.3.rs-1140403/v1

Analytical Study of ZnO-based HEMT for Power Switching

Pawan Kumar[1*], Sumit Chaudhary[1], Md Arif Khan[1], Sanjay Kumar[1] and Shaibal Mukherjee[1,2]

[1]Hybrid Nanodevice Research Group (HNRG), Department of Electrical Engineering, Indian Institute of Technology Indore, Madhya Pradesh, India, 453552.
[2]Centre for Advanced Electronics (CAE), Indian Institute of Technology Indore, Madhya Pradesh, India 453552.

*Corresponding author(s). E-mail(s): phd1701202002@iiti.ac.in;
Contributing authors: Phd1901202011@iiti.ac.in;
mdarif456.khan@gmail.com; phd1701202005@iiti.ac.in;
shaibal@iiti.ac.in;

Abstract

We investigate the power switching mechanism to evaluate the power loss ($\boldsymbol{P_D}$) and efficiency ($\boldsymbol{\eta}$) in MgZnO/ZnO (MZO)-based power high electron mobility transistor (HEMT), and physical parameters responsible for $\boldsymbol{P_D}$ in molecular beam epitaxy (MBE) and dual ion beam sputtering (DIBS) grown MZO HEMT and compare the performance with the group III-nitride HEMTs. This work extensively probes all physical parameters such as two-dimensional electron gas (2DEG) density, mobility, switching frequency, and device dimension to study their impact on power switching in MZO HEMT. Results suggest that the MBE and DIBS grown MZO HEMT with the gate width ($\boldsymbol{W_G}$) of ∼205 and ∼280 mm at drain current coefficient (k) of 11 and 15, respectively, will achieve 99.96 and 99.95% of $\boldsymbol{\eta}$ and 9.03 and 12.53 W of $\boldsymbol{P_D}$, respectively. Moreover, $\boldsymbol{W_G}$ value for DIBS-grown MZO HEMT is observed to further reduce in the range of 112-168 mm by using a $\boldsymbol{Y_2O_3}$ spacer layer leading to the maximum $\boldsymbol{\eta}$ in the range of 99.98-99.97% and the minimum $\boldsymbol{P_D}$ in the range of 5-7 W. This work is significant for the development of cost-effective HEMTs for power switching applications.

Keywords: Efficiency, power dissipation, MgZnO/ZnO HEMT, 2DEG, switching frequency.

1 Introduction

To counter the issue of rising CO_2 emissions, renewable and cost-effective energy sources are [1, 2]in substantial demand. It is well-know that enhancing the system efficiencies of energy conversion and power generation with improved power switching devices and control techniques can significantly contribute towards reduction in energy demand [3]. Solid-state power transistors equipped with high-efficiency power conversion in power electronic converters are one of the prominent solutions for effective energy utilization [4].

Various material systems have been explored to devise efficient power transistors, such as, Si, GaAs etc. As Si and GaAs-based power devices have reached their theoretical limits of power density [3, 5], wide bandgap materials, such as GaN-based high electron mobility transistors (HEMT) are being extensively explored to further push the efficiency and power density limits of power devices [4]. ZnO is another promising wide bandgap material system that displays large energy bandgap (3.37 eV) [6], high breakdown field ($\sim 3MV/cm$) [7], and large saturation drift velocity ($\approx 10^7 cm/s$) [6] and this material system has not been explored extensively for power HEMT applications. ZnO-based heterostructures have shown higher two-dimensional electron gas (2DEG) density ($\sim 10^{13} - 10^{14} cm^{-2}$) [6, 8, 9] than that exhibited in the GaN-based heterostructures, which is one of the crucial parameters to realize high current densities in power HEMTs. In addition, ZnO, as a material, provides unique advantages of high-quality material production at lower temperatures (100 to 300 ℃) using even a cost-effective polycrystalline growth system along with the accessibility to large-area ZnO substrates at relatively low cost [6, 10, 11]. Sasa *et al* [12], Koike *et al* [13], and Ye *et al* [14] have realized high-quality epitaxially-grown MgZnO/ZnO (MZO) based HEMT. Moreover, reports of realizing high 2DEG yielding sputtered [6, 9, 15, 16] MZO heterostructures are available in the literature, suggesting the possibility of achieving large-area and therefore, low-cost ZnO-based power HEMTs.

In this work, we have assumed the operating point (900 V, 30 A) for the evaluation of power device performance parameters essential for the electric vehicle converters, which require a voltage range of 600-900 V and a power rating $>$ 20 kW [17, 18].This work extensively evaluates the power device performance parameters, such as, power dissipation (P_D), power dissipation density (P_{DD}), and power efficiency (η) of MZO HEMT with respect to operating point coefficient of drain current (k), 2DEG density (n_s), and switching frequency (f_s), analytically. The performance of power HEMT is investigated for MZO system realized both by molecular beam epitaxy (MBE) as well as cost-effective sputtering systems. Further, as the electron mobility is one of the important parameters for power transistor application due to its direct

proportionality to the conduction losses of the transistor, this work also qualitatively explores the impact of a thin Y_2O_3 layer as a spacer layer in sputtered MZO heterostructure, as it is observed to enhance the electron mobility in dual ion beam sputtering (DIBS)-grown MgZnO/CdZnO heterostructure [19]. The obtained results suggest that to achieve the minimum value of P_D, a device W_G value of ∼205 and ∼280 mm is necessary for MZO HEMTs grown by MBE and DIBS, respectively. Moreover, the insertion of Y_2O_3 spacer layer in the MZO HEMT further reduces W_G value in the range of 112-168 mm. This work also provides an insight for a device designer to select the optimum k values for the selected f_s while designing a power HEMT. The findings of this work suggest that the DIBS-grown MZO heterostructure can be explored as a cost-effective high-power HEMTs with potential application in power switching devices.

2 ANALYTICAL MODEL FORMULATION

It is known that in switching operation the transistors alternate between ON-state and OFF-state, as shown in fig. 1, where in the ON-state the gate opens the channel and allows the electrons flow through the device while in the OFF-state the gate closes the channel and blocks the current flow. For efficient switching, the OFF-state operation point conditions should be at large positive drain voltage (V_{OFF}) and negligible drain current (I_D), which requires a strong gate blocking capability [20]. However, at a high positive drain voltage (V_D), the gate-blocking capability of the HEMT degrades and gives rise to subthreshold leakage current. It is well-known that the value of V_D at which I_D exceeds the traditional value of drain current density (1 mA/mm) is designated as the breakdown voltage (V_{BR}). For the ON-state, operation point condition should be minimum V_D and maximum I_D (I_{ON}). For safe operation of the HEMT, the operating point (V_{OFF}, I_{ON}) is considered in the present work. As shown in fig. 1, maximum current (I_{max}) and V_{BR} are assumed to be k and S times higher than the values of I_{ON} and V_{OFF}, where k and S are operating point coefficients in the $I_D - V_D$ characteristics.

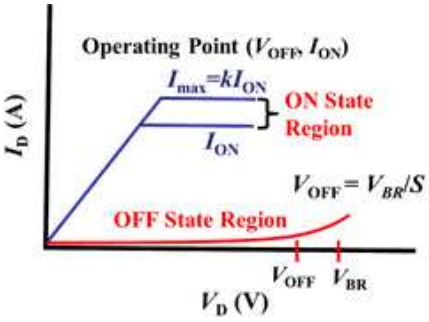

Fig. 1 $I_D - V_D$ characteristics of HEMT for switching operation.

To understand more on power switching efficiency, one needs to investigate the losses that take place in power HEMT. It is well-known that the nonideal behavior of a power switch is described in terms of conduction and switching losses that are analyzed in the next section.

2.1 Conduction Loss

This accounts for the voltage drop across the series resistance from source to drain terminals (contact and sheet resistance) of the transistor, as shown in fig. 2. The sources of the conduction losses are: (a) ON-state nonzero voltage due to the device ON-state resistance (R_{ON}), and (b) OFF-state nonzero current due to the leakage effect. However, the leakage effect (current) is marginal and does not vary significantly with V_D and therefore, it is neglected in this work like others in the published literature [21].

Based on the ON-state resistance, the direct-current (DC) power dissipation becomes [21, 22]:

$$P_{CL} = DI_{On}^2 R_{ON} \tag{1}$$

where, D is the duty cycle. R_{ON} is the sum of sheet resistance (R_{sh}) and the drain and source contact resistance (R_c). Here, the effect of R_c is neglected as the value R_c of is much less as compared to that of R_{sh}. Therefore, R_{ON} is expressed as [21, 22]:

$$R_{ON} = \frac{R_{sh} L_{GD}}{W_G} \tag{2}$$

$$R_{sh} = \frac{1}{q n_s \mu} \tag{3}$$

where, q and μ are the charge and mobility of electron, respectively.

For an estimation of the device dimension, we assume a constant electric field distributed across the drain to gate depletion region and hence, gate to drain length (L_{GD}) can be given by equation (4) [21]. Further, the total gate width (W_G) is calculated in terms of maximum current density (J_{max}) and the operational current bias (I_{ON}). Therefore, W_G can be expressed as in equation (5) [21]:

$$L_{GD} = \frac{S V_{OFF}}{E_{BR}} \tag{4}$$

$$W_G = \frac{k I_{ON}}{J_{max}} \tag{5}$$

where, E_{BR} is the breakdown electrical field. $J_{max} = q n_s v_s$ [23], where v_s is saturation velocity of electron.

2.2 Switching Loss

This occurs during device switching from OFF- to ON-state and vice versa. To calculate the switching losses, gate to drain capacitor (C_{gd})-based model, a schematic of which is shown in fig. 3, is considered. When gate to drain region is in the reverse bias condition, the modulation of the depletion region width (x_d) during the switching operation corresponds to charging and discharging of

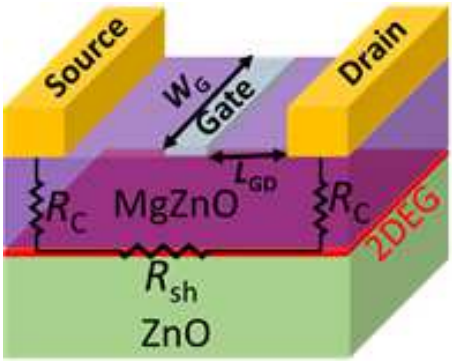

Fig. 2 Schematic of MgZnO/ZnO HEMT with the contribution of series resistance for conduction loss estimation.

C_{gd}. The energy dissipated in each charging and discharging cycle needs to be multiplied by the switching frequency (f_s) to obtain the switching losses [21].

Based on the switching frequency and charge accumulated in between the gate to drain contact, the switching losses can be written as [21, 22]:

$$P_{SL} = V_{off} q n_S x_d W_G f_s \tag{6}$$

where, $x_d = \frac{V_{off}}{E_{br}}$ is the gate to drain depletion region extension in the gate to drain access region.

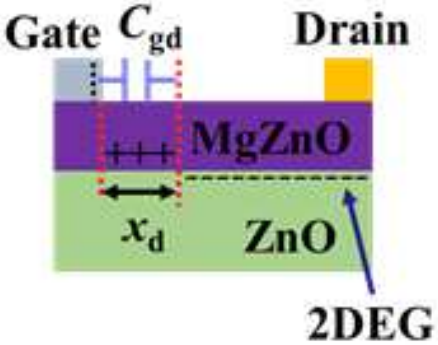

Fig. 3 Schematic of power HEMT for switching loss estimation.

The power dissipation (P_D), being the combination of the conduction and switching losses, can be expressed as:

$$P_D = P_{CL} + P_{SL} \tag{7}$$

In addition, the power efficiency of the HEMT is defined as the ratio of output power (P_{out}) to the summation of P_{out} and P, and can be written as:

$$\eta = \frac{P_{out}}{P_{out} + P_D} \tag{8}$$

where $P_{out} = V_{OFF} I_{ON}$

Further, the power dissipation density (P_{DD}) is considered as the total power loss divided by the active area of power HEMT, as expressed by equation (9) [21, 22]:

$$P_{DD} = \frac{P_D}{W_G L_{GD}} \tag{9}$$

Table 1 Parameters utilized for modelling of GaN and ZnO based heterostructures.

Parameters (unit)	AlGaN/GaN	MBE MZO	DIBS MZO
$n_s(cm^{-2})$	1×10^{13} [24]	1×10^{13} [8]	1×10^{13} [6]
2DEG electron mobility (μ) ($cm^2/V.s$)	1500 [24]	250 [8]	130 [6]

3 RESULTS and DISCUSSION

To fig. 4(a) exhibits the comparative analysis of the variation of P_D and P_{DD} for AlGaN/GaN and MgZnO/ZnO HEMTs with respect to operating point coefficient (k) of I_D. Here, we have assumed $V_{OFF} = 900$ V, $I_{ON} = 30$ A, $f_s = 500$ kHz, duty cycle = 10% for power dissipation calculation, and S = 1.4 for the operation of the device in the safe mode. It is observed that P_D is higher at the lower value of k (k ¡ 5) owing to higher value of R_{ON} which is associated with the higher conduction loss, as per equations (2) and (5). P_D decreases up to certain critical values of k (k = 5) for AlGaN/GaN HEMT, while k = 11 for MBE-grown and 15 for DIBS-grown MZO HEMTs. On the other hand, P_D increases beyond the critical value of k owing to switching losses, as described in equations (5) and (6).

The smallest value of P_D of 3.7 W is observed at k = 5 (W_G = 93 mm) for AlGaN/GaN HEMT and 9.03 and 12.53 W at k = 11 (W_G = 205 mm) and 15 (W_G = 280 mm) for MZO HEMTs grown by MBE and DIBS, respectively. Higher values of P_D in MZO HEMT are mainly due to the lower 2DEG mobility, which leads to the high values of R_{sh} and R_{ON}. In addition to this, large dislocation and alloy disorder scattering also influence the rise in R_{sh} in DIBS grown MZO-based HEMT [25, 26]. The values of P_{DD} at minimum $_D$ are 942 W/cm^2 for AlGaN/GaN HEMT and 1044 and 1062 W/cm^2 for MZO HEMTs by MBE and DIBS, respectively. For increasing k, P_{DD} saturates to 528 W/cm^2 (W_G = 524 mm) for AlGaN/GaN HEMT and 551 and 570 W/cm^2 (W_G = 786 and 880 mm) for MZO HEMT by MBE and DIBS, respectively.

The increase in P_D beyond the critical level of k is mainly because P_S increases with k ($\propto W_G$).

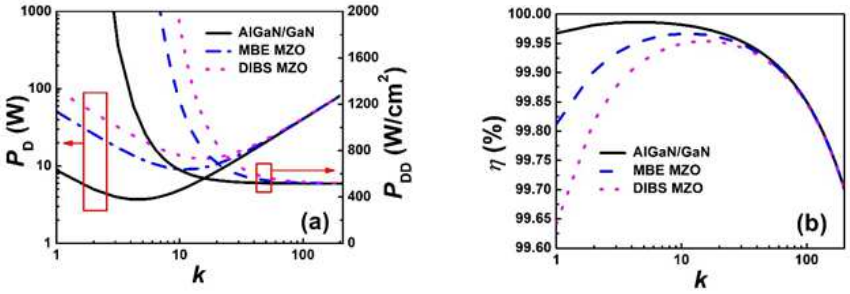

Fig. 4 The variation of (a) P_D and P_{DD}, and (b) η with respect to k for AlGaN/GaN and MgZnO/ZnO HEMTs.

Fig. 4(b) shows the power efficiency of HEMT (η) versus k plot for AlGaN/-GaN and MZO HEMTs. The maximum value of η for AlGaN/GaN HEMT is 99.98% for k = 5 and 99.96% for k = 11 and 99.95% for k = 15 for MBE- and DIBS-grown MZO, respectively. At lower value of k (< 11), the efficiency of MZO power HEMT is low as the conduction losses are higher. However, at higher value of k (> 15), the efficiency is reduced for all power HEMTs as the switching losses play a dominant role.

Fig. 5(a) shows the efficiency of DIBS-grown MZO HEMT as a function of k with different 2DEG density (and 2DEG mobility). Here, four different values of 2DEG density (2DEG mobility) values are considered such as 1×10^{13} (130 $cm^2/V.s$), 5×10^{13} (80 $cm^2/V.s$), 8×0^{13} (40 $cm^2/V.s$), and 1×10^{14} cm^{-2} (28 $cm^2/V.s$). It is observed in fig. 5(a) that the value of η is decreased with rise in 2DEG density from 1×10^{13} to 1×10^{14} cm^{-2} at lower value of k (< 20) as R_{ON} rises with the value of 2DEG density. For k < 20, the conduction losses are increased, however, for higher value of k ($\geq$ 20), the power efficiency is approximately equal for all values of n_s, as evident from equations (1-3). On the other hand, switching losses are not affected by the change in n_s, as observed from equation (5). When n_s increases W_G reduces and overall the value of P_{SL} remains constant.

Fig. 5(b) shows the variation of η with respect to f_s in which three values of f_s is considered such as 500 kHz, 1 MHz, and 5 MHz. The drop in efficiency with increasing k is more prominent for higher values of f_s, as observed from equation (6). At f_s = 1 and 5 MHz, the values of η declines for k > 51 and k > 6, respectively. Inset of fig. 5(b) shows the range of k with respect to different values of f_s for the η_{max} obtained for MZO power HEMT. To design a power HEMT at a specific value of f_s, one can easily evaluate the range of permissible W_G values with respect to the power efficiency.

Khan *et al* [19] have reported the insertion of Y_2O_3 spacer layer between the substrate and CdZnO buffer layer in the DIBS-grown MgZnO/CdZnO

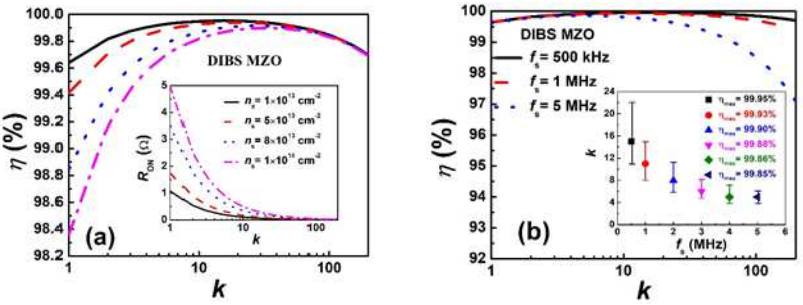

Fig. 5 Power HEMT efficiency as function of k for different (a) 2DEG density and (b) switching frequencies. Insets in fig. 5(a) represents the variation of RON with ns and in fig. 5(b) represents the range of k for different f_s at η_{max} for DIBS-grown MZO power HEMT.

(MCO) HEMT, the 2DEG mobility is enhanced by 6× as compared to that for MCO HEMT without any spacer layer. Even though the lattice matching of Si/ZnO is much better as compared to that for Si/CdZnO, we assume a maximum of 6× enhancement of μ for the DIBS-grown MZO HEMT using Y_2O_3 spacer layer. For this study, 3× or 6× values of μ are assumed for DIBS-grown MZO HEMTs and are presented as MZY1 and MZY2, respectively. The less improvement in μ is assumed considering a maximum of 6× enhancement of μ is not achievable due to the change in experimental parameters.

As observed in fig. 6(a), for MZY2, the minimum value of P_D is ≈ 5 W at k = 6 (W_G = 112 mm) which is very close to the minimum P_D value of AlGaN/GaN HEMT (≈ 3.7 W at k = 5, W_G = 93 mm). For MZY1, the minimum value of P_D is 7 W at k = 9 (W_G = 168 mm). For lower k, the relatively higher values of P_D for MZY2 as compared to that for AlGaN/GaN is due to the higher R_{ON} for MZY2. The values of P_{DD} corresponding to the minimum P_D values are 1022, 1085 W/cm^2 and the P_{DD} curve saturates at 536, 525 W/cm^2 for MZY1 and MZY2, respectively.

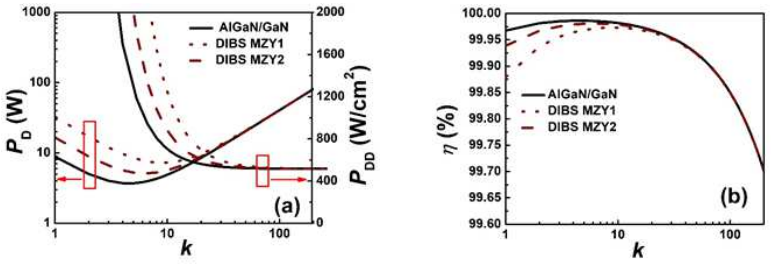

Fig. 6 The variation of (a) P_D and P_{DD}, and (b) η with respect to k for AlGaN/GaN and MZY HEMTs.

Fig. 6(b) shows the comparative analysis of η as a function of k for AlGaN/-GaN and MZY based HEMTs. The maximum value of η (η_{max}) remains at 99.98% for $5 \leq k \leq 8$ for MZY2 HEMT and this value is similar to that for

AlGaN/GaN HEMT. η_{max} remains at 99.97 % for $6 \leq k \leq 14$ for MZY1 HEMT that is 0.01% less than that for MZY2 and AlGaN/GaN HEMTs.

For the 900 V and 30 A power application, W_G for AlGaN/GaN HEMT is evaluated to range from 93 mm (for P_D minimum) to 524 mm (for P_{DD} saturation). Similar experimentally reported values of W_G (200-340 mm) is reported elsewhere for the current range of 20-60 A [27, 28]. At f_s = 500 kHz and duty cycle = 10%, the model predicts 81 W of maximum P_D, as in fig. 4(a), in AlGaN/GaN HEMT and this value is close to the experimental report of 119 W [29]. Similar values of maximum P_D for MBE-grown MZO, and DIBS-grown MZO and MZY HEMTs, as in fig. 4(a), are 82, 97, and 81 W, respectively. Thus, to achieve the comparable power efficiency with minimal power dissipation in MZO HEMT with respect to those for AlGaN/GaN HEMT, one can easily play with DIBS growth parameters and choose a little larger W_G. This, coupled with reduced manufacturing cost of DIBS-grown ZnO-based HEMTs are promising for large-area power switching applications.

4 CONCLUSION

In this work, an analytical model is utilized to investigate the power switching and evaluate the power efficiency and loss parameters of MZO HEMT and compare those with the group III-nitride counterparts. A W_G value of $\sim$ 205 and $\sim$280 mm for MBE- and DIBS-grown MZO HEMT are found to be essential to attain η_{max} of 99.96 and 99.95% and the minimum P_D of 9.03 and 12.53 W, respectively. Moreover, W_G value for DIBS-grown MZO HEMT is observed to further reduce in the range of 112-168 mm by using a Y_2O_3 spacer layer leading to max in the range of 99.98-99.9% and the minimum P_D in the range of 5-7 W. This work also provides an insight on the allowed W_G values while designing a DIBS-grown power HEMT at a fixed f_s with respect to the desired power efficiency. This work is significant while designing a cost-effective DIBS-grown MZO HEMTs for power switching applications.

5 ACKNOWLEDGMENT

Sanjay Kumar would like to thank DST for providing DST-INSPIRE PhD fellowship.

References

[1] Stram, B.N.: Key challenges to expanding renewable energy. Energy Policy **96**, 728–734 (2016). https://doi.org/10.1016/j.enpol.2016.05.034

[2] Babatunde, O.M., Munda, J.L., Hamam, Y.: Power system flexibility: A review. Energy Reports **6**, 101–106 (2020). https://doi.org/10.1016/j.egyr.2019.11.048. The 6th International Conference on Power and Energy Systems Engineering

[3] Ikeda, N., Niiyama, Y., Kambayashi, H., Sato, Y., Nomura, T., Kato, S., Yoshida, S.: Gan power transistors on si substrates for switching applications. Proceedings of the IEEE **98**(7), 1151–1161 (2010). https://doi.org/10.1109/JPROC.2009.2034397

[4] Ding, X., Zhou, Y., Cheng, J.: A review of gallium nitride power device and its applications in motor drive. CES Transactions on Electrical Machines and Systems **3**(1), 54–64 (2019). https://doi.org/10.30941/CESTEMS.2019.00008

[5] Jones, E.A., Wang, F.F., Costinett, D.: Review of commercial gan power devices and gan-based converter design challenges. IEEE Journal of Emerging and Selected Topics in Power Electronics **4**(3), 707–719 (2016). https://doi.org/10.1109/JESTPE.2016.2582685

[6] Singh, R., Khan, M.A., Sharma, P., Htay, M.T., Kranti, A., Mukherjee, S.: Two-dimensional electron gases in MgZnO/ZnO and ZnO/MgZnO/ZnO heterostructures grown by dual ion beam sputtering. Journal of Physics D: Applied Physics **51**(13), 13–02 (2018). https://doi.org/10.1088/1361-6463/aab183

[7] Ding, K., Avrutin, V., Izyumskaya, N., Özgür, , Morkoç, H., Šermukšnis, E., Matulionis, A.: High-performance bemgzno/zno heterostructure field-effect transistors. physica status solidi (RRL) – Rapid Research Letters **14**(12), 2000371 (2020) https://onlinelibrary.wiley.com/doi/pdf/10.1002/pssr.202000371. https://doi.org/10.1002/pssr.202000371

[8] Tampo, H., Shibata, H., Maejima, K., Yamada, A., Matsubara, K., Fons, P., Kashiwaya, S., Niki, S., Chiba, Y., Wakamatsu, T., Kanie, H.: Polarization-induced two-dimensional electron gases in znmgo/zno heterostructures. Applied Physics Letters **93**(20), 202104 (2008) https://doi.org/10.1063/1.3028338. https://doi.org/10.1063/1.3028338

[9] Chin, H.-A., Cheng, I.-C., Huang, C.-I., Wu, Y.-R., Lu, W.-S., Lee, W.-L., Chen, J.Z., Chiu, K.-C., Lin, T.-S.: Two dimensional electron gases in polycrystalline mgzno/zno heterostructures grown by rf-sputtering process. Journal of Applied Physics **108**(5), 054503 (2010) https://doi.org/10.1063/1.3475500. https://doi.org/10.1063/1.3475500

[10] Siddharth, G., Singh, R., Garg, V., Sengar, B.S., Das, M., Mandal, B., Htay, M.T., Gupta, M., Mukherjee, S.: Investigation of dibs-deposited cdzno/zno-based multiple quantum well for large-area photovoltaic application. IEEE Transactions on Electron Devices **67**(12), 5587–5592 (2020). https://doi.org/10.1109/TED.2020.3031235

[11] Awasthi, V., Pandey, S.K., Kumar, S., Mukherjee, C., Gupta, M.,

Mukherjee, S.: Evaluation of the band alignment and valence plasmonic features of a DIBS grown ga-doped mg0.05zn0.95o/CIGSe heterojunction by photoelectron spectroscopy. Journal of Physics D: Applied Physics **48**(48), 485305 (2015). https://doi.org/10.1088/0022-3727/48/48/485305

[12] Sasa, S., Maitani, T., Furuya, Y., Amano, T., Koike, K., Yano, M., Inoue, M.: Microwave performance of zno/znmgo heterostructure field effect transistors. physica status solidi (a) **208**(2), 449–452 (2011) https://onlinelibrary.wiley.com/doi/pdf/10.1002/pssa.201000509. https://doi.org/10.1002/pssa.201000509

[13] Koike, K., Nakashima, I., Hashimoto, K., Sasa, S., Inoue, M., Yano, M.: Characteristics of a zn0.7mg0.3ozno heterostructure field-effect transistor grown on sapphire substrate by molecular-beam epitaxy. Applied Physics Letters **87**(11), 112106 (2005) https://doi.org/10.1063/1.2045558. https://doi.org/10.1063/1.2045558

[14] Ye, D., Mei, Z., Liang, H., Li, J., Hou, Y., Gu, C., Azarov, A., Kuznetsov, A., Hong, W.-C., Lu, Y., Du, X.: Enhancement-mode ZnO/mg0.5zn0.5o HFET on si. Journal of Physics D: Applied Physics **47**(25), 255101 (2014). https://doi.org/10.1088/0022-3727/47/25/255101

[15] Wang, B.-S., Li, Y.-S., Cheng, I.-C.: Mobility enhancement in rf-sputtered mgzno/zno heterostructure thin-film transistors. IEEE Transactions on Electron Devices **63**(4), 1545–1549 (2016). https://doi.org/10.1109/TED.2016.2526649

[16] Hwang, J.D., Chu, C.M.: Post oxidation in improving the schottky-gate mgzno/zno heterojunction field-effect transistors fabricated by rf sputtering. Materials Science and Engineering: B **266**, 115063 (2021). https://doi.org/10.1016/j.mseb.2021.115063

[17] Roccaforte, F., Greco, G., Fiorenza, P., Iucolano, F.: An overview of normally-off gan-based high electron mobility transistors. Materials **12**(10) (2019). https://doi.org/10.3390/ma12101599

[18] Shen, Z.J., Omura, I.: Power semiconductor devices for hybrid, electric, and fuel cell vehicles. Proceedings of the IEEE **95**(4), 778–789 (2007). https://doi.org/10.1109/JPROC.2006.890118

[19] Khan, M.A., Kumar, P., Das, M., Htay, M.T., Agarwal, A., Mukherjee, S.: Drain current optimization in dibs-grown mgzno/cdzno hfet. IEEE Transactions on Electron Devices **67**(6), 2276–2281 (2020). https://doi.org/10.1109/TED.2020.2989731

[20] Bahat-Treidel, E.: Gan based hemts for high voltage operation. design,

technology and characterization. Doctoral thesis, Technische Universität Berlin, Fakultät IV - Elektrotechnik und Informatik, Berlin (2012). https://doi.org/10.14279/depositonce-3203. http://dx.doi.org/10.14279/depositonce-3203

[21] Esposto, M., Chini, A., Rajan, S.: Analytical model for power switching gan-based hemt design. IEEE Transactions on Electron Devices **58**(5), 1456–1461 (2011). https://doi.org/10.1109/TED.2011.2112771

[22] Kumar, S., Soman, R., Pratiyush, A.S., Muralidharan, R., Nath, D.N.: A performance comparison between ¡inline-formula¿ ¡tex-math notation="latex"¿β ¡/tex-math¿¡/inline-formula¿-ga¡sub¿2¡/sub¿o¡sub¿3¡/sub¿ and gan hemts. IEEE Transactions on Electron Devices **66**(8), 3310–3317 (2019). https://doi.org/10.1109/TED.2019.2924453

[23] Fang, T., Wang, R., Xing, H., Rajan, S., Jena, D.: Effect of optical phonon scattering on the performance of gan transistors. IEEE Electron Device Letters **33**(5), 709–711 (2012). https://doi.org/10.1109/LED.2012.2187169

[24] Kumar, S., Gupta, P., Guiney, I., Humphreys, C.J., Raghavan, S., Muralidharan, R., Nath, D.N.: Temperature and bias dependent trap capture cross section in algan/gan hemt on 6-in silicon with carbon-doped buffer. IEEE Transactions on Electron Devices **64**(12), 4868–4874 (2017). https://doi.org/10.1109/TED.2017.2757516

[25] Kumar, P., Khan, M.A., Siddharth, G., Kumar, S., Singh, R., Mukherjee, S.: Electron scattering analysis in 2deg in sputtering-grown MgZnO/ZnO heterostructure. Journal of Physics D: Applied Physics **53**(12), 125108 (2020). https://doi.org/10.1088/1361-6463/ab6467

[26] Li, Q., Zhang, J., Zhang, Z., Li, F., Hou, X.: Electron transport in ZnMgO/ZnO heterostructures. Semiconductor Science and Technology **29**(11), 115001 (2014). https://doi.org/10.1088/0268-1242/29/11/115001

[27] Kambayashi, H., Kamiya, S., Ikeda, N., Li, J., Kato, S., Ishii, S., Sasaki, Y., Yoshida, S., Masuda, M.: Improving the performance of gan power devices for high breakdown voltage and high temperature operation. (2008)

[28] Ikeda, N., Kaya, S., Li, J., Kokawa, T., Satoh, Y., Katoh, S.: High-power algan/gan hfets on si substrates. In: The 2010 International Power Electronics Conference - ECCE ASIA -, pp. 1018–1022 (2010). https://doi.org/10.1109/IPEC.2010.5542033

[29] TP90H050WS, T.I.: Goleta, CA, USA, pp. 1–12, July 2020. Available:.

https://www.transphormusa.com